Dalton Transactions

PAPER

View Article Online
View Journal | View Issue

Cite this: *Dalton Trans.*, 2017, **46**, 10408

Sensitization of NIR luminescence of Yb^{3+} by Zn^{2+} chromophores in heterometallic complexes with a bridging Schiff-base ligand†

Anatoly P. Pushkarev, *[a,b] Tatyana V. Balashova,[a] Andrey A. Kukinov,[c] Maxim V. Arsenyev, [a,c] Artem N. Yablonskiy,[c,d] Denis I. Kryzhkov,[c,d] Boris A. Andreev, [c,d] Roman V. Rumyantcev,[a] Georgy K. Fukin[a] and Mikhail N. Bochkarev*[a,c]

Received 13th April 2017,
Accepted 4th July 2017

DOI: 10.1039/c7dt01340j

rsc.li/dalton

Herein, complexes $[ZnL]_2$ (**1**), $\{(H_2O)Zn(\mu\text{-}L)Yb[OCH(CF_3)_2]_3\}$ (**2**), $\{[(CF_3)_2HCO]Zn(\mu\text{-}L)Yb[OCH(CF_3)_2](\mu\text{-}OH)\}_2$ (**3**), and $[(H_2O)Ln_2(L)_3]$ (Ln = Yb (**4**) and Gd (**5**)) containing a bridging Schiff-base ligand (H_2L = *N*,*N*′-bis(3-methoxy salicylidene)phenylene-1,2-diamine) were synthesized. The compounds **1–4** were structurally characterized. The ytterbium derivatives **2–4** exhibited bright NIR metal-centred photoluminescence (PL) of Yb^{3+} ion under one- (λ_{ex} = 380 nm) and two-photon (λ_{ex} = 750 nm) excitation. The superior luminescence properties of complex **2**, which was suggested as a marker for NIR bioimaging, were explained *via* the strong absorption of the 375 nm LMCT state of the ZnL chromophore, efficient energy transfer from ZnL towards Yb^{3+} through a reversible ligand-to-lanthanide electron transfer process, and absence of luminescence quenchers (C–H and O–H groups) in the first coordination sphere of the rare-earth atom.

Introduction

Discovered more than half a century ago, nowadays, lanthanides have undoubtedly become a part of sustainable living owing to their broad practical applications such as in strong magnets, active (lasers and fiber amplifiers) and passive (LEDs, OLEDs, PVs, and OPVs) optoelectronic devices, phosphors for white lighting, and biomedical imaging.[1–7] Except lanthanum and lutetium, Ln^{3+} ions are able to generate long-lived line-like f–f emission in response to direct photoexcitation at metal absorption bands or energy transfer from excited states of sensitizing ligands. These features, along with reduced scattering of near-infrared (NIR) light in the biological media, make lanthanide-based materials, emitting in the first biological transparency window (λ = 700–1100 nm), very attractive for in-depth, time-gated imaging of thick tissues. For this purpose, Nd, Sm, and Yb complexes are potentially well-suited in combination with a two-photon (2P) excitation technique and signal registration at a wavelength longer than the incident laser pulse wavelength.[8–11] Since signal-to-noise ratio *versus* laser power has quadratic dependence in this case and a common source of two-photon sensitization is a femtosecond Ti:sapphire laser, which operates most efficiently in the 740–800 nm range, it is of great importance to design lanthanide complexes that exhibit both two-photon absorption bands in the 370–400 nm spectral region and intensive NIR radiation.

A promising strategy for the synthesis of rare-earth derivatives extending their absorption in the visible region is binding of Ln^{3+} ions to d-block metal chromophores (*e.g.* Cr^{3+},[12] Zn^{2+},[13] Ru^{2+},[14] Pt^{2+},[15] and Ir^{3+} (ref. 16)). These chromophores successfully harvest visible light due to severe absorbing singlet and triplet ligand-to-metal (LMCT) or metal-to-ligand (MLCT) charge transfer states and efficiently transmit energy to emissive levels of f-block metals. A ZnL complex with a salen-type Schiff-base ligand (H_2L = *N*,*N*′-bis(3-methoxy salicylidene)phenylene-1,2-diamine) has been reported as one of the possible d-metal units suitable for the design of d–f hetero-

[a]*G. A. Razuvaev Institute of Organometallic Chemistry of Russian Academy of Sciences, Tropinina 49, 603950 Nizhny Novgorod, Russian Federation. E-mail: anatoly.pushkarev@gmail.com, mboch@iomc.ras.ru; Fax: +7 (831) 4627497; Tel: +7 (831) 4627709*
[b]*Department of Nanophotonics and Metamaterials, ITMO University, 197101 St. Petersburg, Russian Federation*
[c]*Nizhny Novgorod State University, Gagarina avenue 23/2, 603950 Nizhny Novgorod, Russian Federation*
[d]*Institute for Physics of Microstructures of Russian Academy of Sciences, 7 ul. Akademicheskaya, 603950 Nizhny Novgorod, Russian Federation*

†Electronic supplementary information (ESI) available: Details of crystallographic, collection and refinement data for **1–4**, PL spectra of **1–5** and energy diagram for **2–5**. CCDC 1537230–1537232. For ESI and crystallographic data in CIF or other electronic format see DOI: 10.1039/c7dt01340j

nuclear compounds and sensitization of metal-centred luminescence.[17–22] Because of compartmental nature of the ligand, Zn^{2+} and Ln^{3+} centres could be allocated to its inner N_2O_2 and outer O_4 cavities, respectively; this yielded various single- and double-decker structures or molecules with ZnL fragments arranged in a crosswise fashion depending on the reaction stoichiometry and presence of other anionic or neutral ligands during the synthesis. Thereby, a number of Nd,[17–20] Eu,[21] Tb,[21,22] and Yb[20] complexes were established to reveal the f–f luminescence, whereas Dy[23] complexes were found to be high performance single-ion magnets. In addition to the existing NIR-emissive Nd and Yb compounds, there is a study reported by Pasatoiu *et al.* that describes two-photon (λ_{ex} = 775)-induced photoluminescence (PL) of Zn–Tb and Zn–Sm heterobimetallic compounds comprising a salen-type ligand with a 2,2-dimethyl-1,3-propanediyl linker.[24] All the abovementioned findings provide a research background for a study on the application of Zn–Ln salen-derived probes in bioimaging.

Herein, we present synthesis, structures, and photophysical properties of the complexes $[ZnL]_2$ (**1**), $\{(H_2O)Zn(\mu\text{-}L)Yb[OCH(CF_3)_2]_3\}$ (**2**), $\{[(CF_3)_2HCO]Zn(\mu\text{-}L)Yb[OCH(CF_3)_2](\mu\text{-}OH)\}_2$ (**3**), and $[(H_2O)Ln_2(L)_3]$ (Ln = Yb (**4**) and Gd (**5**)). Their optical characteristics in the solid state and MeCN solution were determined *via* steady-state and time-resolved spectroscopic techniques. Moreover, the role of Zn-containing chromophore in sensitization of Yb^{3+} emission in response to one- and two-photon excitation has been discussed.

Experimental

General procedures

All manipulations were conducted under vacuum using a Schlenk line technique. Solvents were purified by distillation over sodium/benzophenone ketyl (DME) and calcium hydride. (MeCN). $HOCH(CF_3)_2$ was purchased from a commercial supplier. Ligand H_2L was synthesized *via* a condensation reaction of *o*-vanillin and *o*-phenylenediamine in MeOH. The complexes $Ln[N(SiMe_3)_2]_3$ (Ln = Gd and Yb) and $\{(DME)Yb[OCH(CF_3)_2]_3\}_2$ were synthesized according to the procedures reported in literature.[25,26] The C, H, and N elemental analyses were performed using a Vario EL cube analyzer. Metal content in the compounds $[(H_2O)Ln_2(L)_3]$ (Ln = Gd and Yb) was analyzed *via* complexometric titration. IR spectra were obtained using a PerkinElmer 577 spectrometer in the 4000–450 cm^{-1} region as a Nujol mull on KBr plates. UV-vis absorption spectroscopy was performed in a 1 cm quartz cuvette using a PerkinElmer Lambda-25 from 200 to 700 nm; excitation and emission spectra were obtained *via* PerkinElmer LS-55 in the 200–700 nm range. Emission spectra in the NIR range were obtained using an Ocean Optics NIR512 spectrometer.

Synthesis

$[ZnL]_2$ (1). A solution of $Zn(Et)_2$ (49 mg, 0.40 mmol) in MeCN (5 ml) was added to a solution of H_2L (149 mg, 0.40 mmol) in MeCN (5 ml). The solvent was partially removed by evaporation to obtain an orange crystalline precipitate that was further separated by decantation, washed with cold MeCN, and dried *in vacuo*. Yield 143 mg (82%). Anal. Calcd (%) for $C_{44}H_{36}N_4O_8Zn_2$ (879.60): C, 60.08; H, 4.13; N, 6.37. Found (%): C, 60.11; H, 4.19; N, 6.42. IR (ν, cm^{-1}): 1614 (s), 1586 (m), 1541 (w), 1338 (w), 1241 (s), 1194 (m), 1108 (w), 1076 (w), 981 (w), 864 (w), 759 (w), 727 (s), 628 (w), 586 (w), 541 (w).

$\{(H_2O)Zn(\mu\text{-}L)Yb[OCH(CF_3)_2]_3\}$ (2). A solution of cold, degassed H_2O (3.3 mg, 0.183 mmol) in MeCN (5 mL) was added to a suspension of **1** (82 mg, 0.093 mmol) in MeCN (5 ml). The mixture was stirred at room temperature for 1 h. Then, a solution of $\{(DME)Yb_2[OCH(CF_3)_2]_3\}_2$ (142 mg, 0.093 mmol) in MeCN (5 ml) was added dropwise over 5 min to the mixture. The resulting mixture was stirred at room temperature for 1 h and finally filtered to separate the solution from the residual poorly soluble **1**. The solution was concentrated *via* partial evaporation of the solvent to afford a pale yellow crystalline precipitate that was further separated by decantation, washed with cold MeCN, and dried *in vacuo*. Yield 159.6 mg (76%). Anal. Calcd (%) for $C_{31}H_{23}F_{18}N_2O_8YbZn$ (1131.94): C, 32.89; H, 2.05; N, 2.47. Found (%): C, 32.80; H, 2.09; N, 2.49. IR (ν, cm^{-1}): 3240 (br), 1616 (s), 1587 (m), 1551 (m), 1382 (m), 1315 (m), 1286 (m), 1228 (s), 1190 (s), 1183 (s), 1093 (m), 968 (m), 882 (w), 843 (m), 781 (w), 738 (m), 685 (m), 648 (w), 561 (w).

$\{[(CF_3)_2HCO]Zn(\mu\text{-}L)Yb[OCH(CF_3)_2](\mu\text{-}OH)\}_2$ (3). A solution of cold, degassed H_2O (3.5 mg, 0.194 mmol) in MeCN (5 mL) was added to a suspension of **1** (86 mg, 0.098 mmol) in MeCN (5 ml). The mixture was stirred at room temperature for 1 h. Then, a solution of $\{(DME)Yb_2[OCH(CF_3)_2]_3\}_2$ (150 mg, 0.098 mmol) in MeCN (5 ml) was added dropwise over 5 min to the mixture. The resulting mixture was stirred at 80 °C for 2 h and finally filtered to separate a solution from the residual **1**. The solution was slowly cooled down to room temperature and concentrated *via* partial evaporation of the solvent to obtain a yellow crystalline precipitate that was further separated by decantation, washed with cold MeCN, and dried *in vacuo*. Yield 139 mg (65%). Anal. Calcd (%) for $C_{56}H_{42}F_{24}N_4O_{14}Yb_2Zn_2$ (1927.81): C, 34.89; H, 2.20; N, 2.91. Found (%): C, 34.97; H, 2.26; N, 2.98. IR (ν, cm^{-1}): 3350 (br), 1617 (s), 1584 (m), 1548 (m), 1310 (m), 1283 (m), 1224 (s), 1191 (s), 1173 (s), 1093 (m), 967 (m), 878 (w), 828 (w), 787 (w), 741 (s), 681 (w), 646 (w), 556 (w), 515 (w).

$[(H_2O)Yb_2(L)_3]$ (4). A solution of $Yb[N(SiMe_3)_2]_3$ (20 mg, 0.031 mmol) in DME (10 ml) was added to a solution of H_2L (17 mg, 0.045 mmol) in DME (5 ml). An orange crystalline precipitate was immediately formed. The product was separated by decantation, washed with cold DME, and dried *in vacuo*. Yield 14 mg (61%). Anal. Calcd (%) for $C_{66}H_{56}N_6O_{13}Yb_2$ (1487.24): C, 53.30; H, 3.80; N, 5.65; Yb, 23.27. Found (%): C, 53.34; H, 3.77; N, 5.63; Yb, 23.20. IR (ν, cm^{-1}): 3240 (br), 1612 (s), 1582 (m), 1543 (m), 1378 (s), 1260 (m), 1240 (s), 1200 (m), 1105 (m), 1080 (m), 1022 (m), 980 (w), 857 (w), 838 (w), 804 (m), 732 (s).

$[(H_2O)Gd_2(L)_3]$ (5). Complex **5** was obtained as an orange crystalline precipitate in a similar fashion as **4** from

$Gd[N(SiMe_3)_2]_3$ (60 mg, 0.094 mmol) and H_2L (53 mg, 0.141 mmol) in DME (15 ml). Yield: 47 mg (69%). Anal. Calcd (%) for $C_{66}H_{56}Gd_2N_6O_{13}$ (1455.68): C, 54.46; H, 3.88; N, 5.77; Gd, 21.60. Found (%): C, 54.49; H, 3.85; N, 5.73; Gd, 21.61. IR spectrum of **5** is identical to that of **4**.

X-ray crystallography

The X-ray diffraction data for **1–4** were obtained using Bruker AXS SMART APEX (**1** and **2**) and Oxford Xcalibur Eos (**3** and **4**) diffractometers (Mo-K_α radiation, ω-scan technique, and λ = 0.71073 Å). The intensity data were integrated by SAINT (**1** and **2**) and CrysAlisPro (**3** and **4**) programs.[27,28] All structures were solved by the dual method[29] and refined on F_{hkl}^2 using the SHELXTL package.[30] All non-hydrogen atoms were anisotropically refined. Hydrogen atoms were placed at the calculated positions and refined in the riding-model ($U_{iso}(H) = 1.5U_{eq}(C)$ in CH_3-groups and $U_{iso}(H) = 1.2U_{eq}(C)$ in other ligands). SADABS (**1** and **2**) and SCALE3 ABSPACK (**3** and **4**) were used to perform absorption corrections.[31,32] The crystal of **3** contains solvate molecules of acetonitrile. The main crystallographic data and structure refinement details for **1–4** are presented in Table S1.† CCDC 1537232 (**1** and **2**), 1537231 (**3**), and 1537230 (**4**)† contain the supplementary crystallographic data for this study.

Time-resolved and two-photon spectroscopy

The PL decay times were measured under pulsed excitation with a third harmonic of a Spectra-Physics Nd:YAG laser at 355 nm (pulse duration – 10 ns). The PL signal was dispersed using a grating spectrometer Acton-2300 and detected using a cooled InP/InGaAs-based PMT Hamamatsu H10330A-75 in the 900–1500 nm range. Moreover, two-photon excitation (λ_{ex} = 750 nm) of NIR emission of **2–4** was performed using a Tsunami Spectra-Physics Ti:Sa laser (pulse duration – 120 fs and repetition frequency – 80 MHz). The laser beam spot size at the focal plane was approximately 5 μm. To filter out the laser radiation from the PL signal, an interference filter cutting off wavelengths below 850 nm was exploited. The PL signal was dispersed using a TriVista Princeton Instruments spectrometer and detected by silicon CCD from Princeton Instruments.

Results and discussion

Synthesis

The complex $[ZnL]_2$ (**1**) was obtained as an orange crystalline precipitate *via* the reaction of H_2L with two equivalents of $Zn(Et)_2$ in MeCN. According to the single crystal X-ray analysis data, **1** is a double-decker molecule having unoccupied outer O_4 cavities of the ligands. To produce heterometallic d–f complexes with Yb^{3+} located in the outer O_4 compartment of L^{2-}, a simple strategy of mixing the products **1** and $\{(DME)Yb[OCH(CF_3)_2]_3\}_2$ [26] in MeCN was adopted. The latter precursor has been selected for the following reasons: (i) hexafluoro-isopropoxide groups do not sensitize the luminescence of Yb^{3+}; hence, the sensitization effect can be clearly referred to the ZnL → Yb energy transfer; (ii) $OCH(CF_3)_2^-$ ligands contain minimum C–H oscillators, which are known NIR emission quenchers; (iii) $\{(DME)Yb[OCH(CF_3)_2]_3\}_2$ is most likely capable of dissociating when it reacts with a zinc dimer because its Yb atoms have unfilled coordination sphere (coordination number is 6) and bear sterically non-hindering ligands that are unable to shield the metal centers from the capturing polydentate ZnL chromophore. It has been reported that in the related d–f derivatives, the fifth axial coordination site of Zn^{2+} can be occupied by various neutral ligands (such as aqua,[18,24] acetonitrile,[17] and pyridine[20]). Since during bioimaging, a luminescent marker inevitably interacts with water molecules, it is reasonable to introduce H_2O as a neutral ligand to saturate the coordination spheres of metal atoms in the complexes. In this way, the mixture of two equivalents of aqua, **1**, and $\{(DME)Yb[OCH(CF_3)_2]_3\}_2$ in MeCN was stirred at room temperature for 1 h to afford a pale yellow crystalline precipitate, $\{(H_2O)Zn(\mu\text{-}L)Yb[OCH(CF_3)_2]_3\}$ (**2**).

Suitable for X-ray analysis, the crystals containing molecules of both **1** and **2** within one unit cell were obtained from the similar reaction in which double excess of **1** was exploited. Heating of the former mixture at 80 °C for 2 h resulted in the formation of yellow crystals of $\{[(CF_3)_2HCO]Zn(\mu\text{-}L)Yb[OCH(CF_3)_2](\mu\text{-}OH)\}_2$ (**3**). To compare the contribution of the ZnL chromophore antenna towards the sensitization of Yb^{3+} NIR emission with that of the L^{2-} ligand, a homometallic dinuclear product, $[(H_2O)Yb_2(L)_3]$ (**4**), was prepared *via* the reaction of Yb $[N(SiMe_3)_2]_3$ with H_2L in DME in the presence of water. Since the first triplet excited state is commonly recognized to be a key mediator in the energy transfer between an organic ligand and a rare-earth ion, a gadolinium analogue, (**5**), was synthesized in a similar fashion for the determination of the $^3T_1$ energy level of the ligand. The compounds **1–5** are air- and moisture-stable and have poor (**1**, **4**, and **5**) or moderate (**2** and **3**) solubility in MeCN and DMSO solvents. Schematic of the reactions is depicted in Scheme 1.

Description of the structures

The structural unit of the crystals containing complexes **1** and **2** consists of two neutral heterometallic Yb–Zn molecules (Fig. 1a) between which a dimer molecule $[ZnL]_2$ (Fig. 1b) is disposed. The relatively soft Zn^{2+} ion is located in the inner N_2O_2 cavity and the hard Yb^{3+} ion in the outer O_2O_2 cavity of the L^{2-} ligand. Ytterbium cation is coordinated by four oxygen atoms of the Schiff-base and three oxygen atoms of the isopropoxide groups. As a result, the coordination number of the Yb atom is equal to seven, and its coordination environment is distorted pentagonal bipyramid. The zinc atom in molecule **2** has a distorted tetragonal pyramidal coordination. It deviates from the basal plane (O(2)O(3)N(1)N(2)) of a tetragonal pyramid by 0.694 Å. The Yb–O($OCH(CF_3)_2$) distances lie in the narrow range of 2.131(2)–2.135(2) Å and are in agreement with the analogous distances in other ytterbium complexes.[26,33] As expected, the bridging Yb–μ_2-O(2 and 3) distances (2.293(2)–2.310(2) Å) notably exceed the terminal Yb–O($CH(CF_3)_2$) dis-

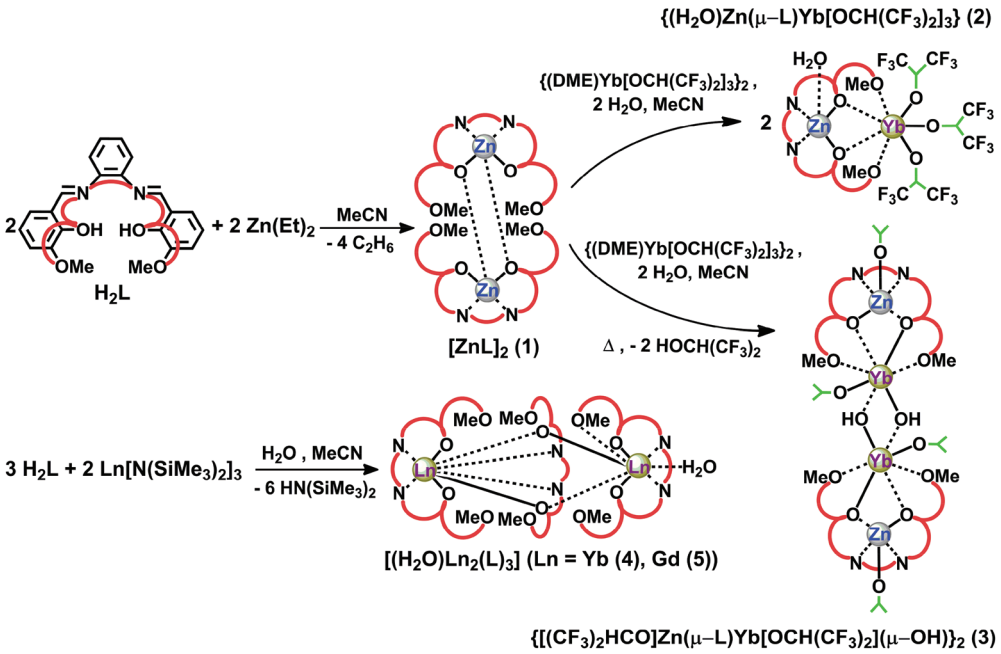

Scheme 1 Synthesis of complexes **1**–**5**.

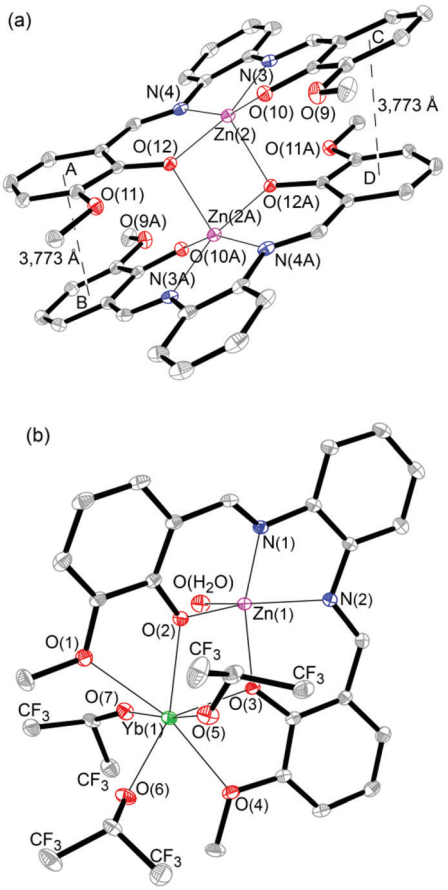

Fig. 1 Molecular structures of **1** (a) and **2** (b). Thermal ellipsoids are drawn at the 30% probability level. H atoms are omitted for clarity.

tances. In turn, the Yb(1)–O(methoxy) distances are maximal (2.547(2) and 2.566(2) Å) as compared to other Yb–O bond lengths in this molecule. The Zn(1)–O(2 and 3) and Zn(1)–N(1 and 2) distances are equal to 2.028(2) and 2.036(2) and 2.065(2) and 2.065(2) Å, respectively. The Zn(1)···O(8) (H_2O) distance (2.002(2) Å) is slightly shorter than the Zn(1)–O(2 and 3) bond lengths. The structure of the heterometallic fragment is typical for related dinuclear Zn(μ-Schiff-base)Ln complexes [(C_5H_5N)Zn(μ-Schiff-base)Nd$(NO_3)_3$], [(MeCN)Zn(μ-Schiff-base)Nd$(NO_3)_3$], and [(H_2O)Zn(μ-Schiff-base)Sm$(NO_3)_3$].[17,34,35] All Zn–O, Zn–N, and Yb···Zn distances are in the normal range and comparable to those of other dinuclear Zn(μ-Schiff-base)Ln complexes.[17,34–36] The shortest Yb···F distance in the bimetallic Yb–Zn molecule is 3.713 Å that exceeds the sum of R(Yb^{3+}) = 0.925 Å (ref. 37) and R(F)vdW = 1.4 Å.[38] The metal centres of the $[ZnL]_2$ (**1**) structural unit have a distorted tetragonal pyramidal coordination, as with the molecule **2**. The Zn atoms deviate from the basal plane of the tetragonal pyramid by 0.273 Å. The Zn(2)O(12)Zn(2A)O(12A) fragment is centrosymmetric. The Zn–O and Zn···Zn distances inside this fragment are 2.030(2) and 2.118(2) and 2.9913(7) Å, respectively. These distances agree with the analogous distances in related dimeric complexes.[39,40] The main geometrical parameters of the dimer molecule are close to the analogous parameters in the ZnL fragment of the Yb–Zn molecule. It is worth noting that the Zn–μ_2-O distance in **1** (2.1180(19) Å) is slightly longer than the Zn–O(H_2O) (2.002(2) Å) distance in the Zn(μ-L)Yb fragment. As distinct from the Zn(2)O(12)Zn(2A)O(12A) fragment of **1**, the Yb(1)O(2)Zn(1)O(3) metallocycle in **2** is not planar. The dihedral angles between the YbOO and ZnOO planes are equal to 17.43°. It should be noted that the ligands in the zinc dimer are parallel to each other. The rings A–B and C–D are

offset to each other, and the distance between the centres of these rings is 3.733 Å, which satisfies the criterion of the presence of π–π interaction between them.[41]

Moreover, two molecules of **2** and one molecule of **1** are combined *via* hydrogen bonds between H_2O molecules and oxygen atoms of the salen-type ligand (Fig. 2). The intermolecular O···H distances are in the 1.94–2.14 Å range and reflect a specific interaction between **1** and **2**.[42]

According to the X-ray data, complex **3** is a heterometallic tetranuclear compound. Herein, two Zn(μ-L)Yb fragments are connected *via* two μ_2-OH^- anions (Fig. 3a and b). As distinct from the Yb(1)O(13)Yb(2)O(14) fragment (the dihedral angles between YbOO planes is 9.01°), the Yb(1)O(1)Zn(1)O(3) and Yb(2)O(7)Zn(2)O(9) metallocycles in **3** are not planar. The dihedral angles between the YbOO and ZnOO planes are equal to 31.64 and 25.21°. Similar to the case of complex **2**, the Yb and Zn atoms in **3** have distorted pentagonal bipyramidal and tetragonal pyramidal coordinations, respectively. The Yb–O, Zn–O, and Zn–N distances vary in the ranges of 2.0895(15)–2.5502(14), 1.9291(15)–2.0270(14), and 2.0449(17)–2.0575(17) Å, respectively. The Yb–O(methoxy) distances are maximal (2.4796(14)–2.5502(14) Å) as compared to other Yb–O bond lengths in **3** as well as in complex **2**. Overall, the geometric parameters in **3** are close to the analogous parameters in the complex **2**. It should be noted that one of the Schiff-bases at the Zn(1) atom has a planar conformation, whereas the other has a butterfly conformation. The dihedral angles between benzene rings connected with oxygen atoms are equal to 4.43° for planar conformation and 23.14° for butterfly conformation. The Yb–OH distances (2.1590(14)–2.2356(14) Å) and Yb(1)···Yb(2) (3.53628(12) Å) in **3** perfectly agree with the corresponding distances in the related Ni–Yb tetrameric complex.[43]

Complex **4** has a dimeric structure containing two Yb^{3+} ions, two terminal and one bridging Schiff-bases, as well as an additionally coordinated H_2O molecule (Fig. 4). The molecular structure of **4** is similar to that of the related compound

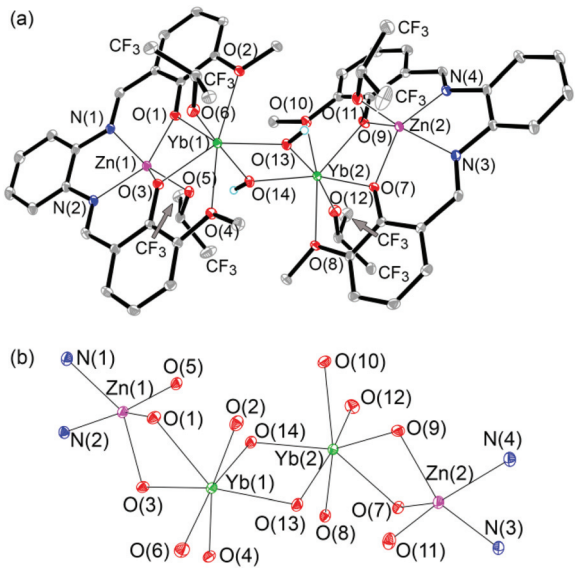

Fig. 3 Molecular structure of **3** (a) and the central core (b). Thermal ellipsoids are drawn at the 30% probability level. H atoms are omitted for clarity.

$[(CH_3OH)Yb_2L_3]$.[44] Contrary to those in the complexes **2** and **3**, the ytterbium atoms in **4** are located in the N_2O_2 cavity of the terminal L^{2-} ligands. The Yb(1) cation is coordinated by four heteroatoms of the terminal ligand and four heteroatoms of the bridging Schiff-base. Thereby, the coordination environment of the Yb(1) cation is a distorted square antiprism, and the coordination number is equal to eight. In addition, another Yb^{3+} ion is coordinated by four heteroatoms of one terminal ligand and only two oxygen atoms of the bridging ligand. Moreover, the Yb(2) atom is bound to the H_2O molecule. It is important to note that the distance between the Yb(2) atom and oxygen of one methoxy group (O(8)) of the bridging ligand (3.056(2) Å) is significantly shorter than others

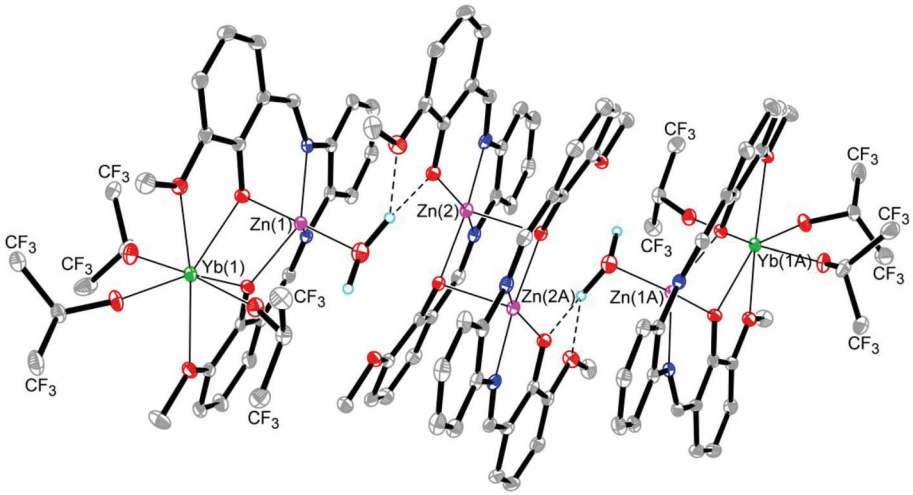

Fig. 2 Structural unit consisting of one molecule of **1** and two **2** molecules combined *via* hydrogen bonds. Thermal ellipsoids are drawn at the 15% probability level. The H and F atoms are omitted for clarity.

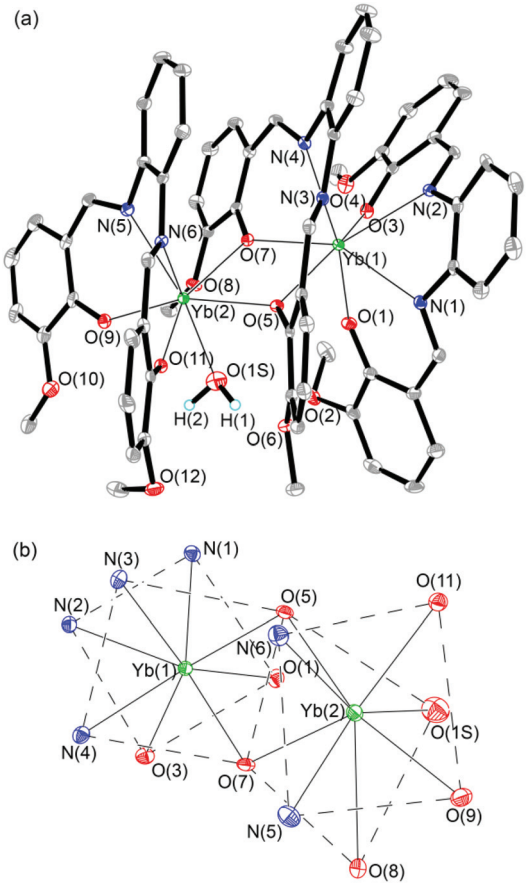

Fig. 4 Molecular structure of **4** (a) and the central core (b). Thermal ellipsoids are drawn at the 30% probability level. H atoms are omitted for clarity.

(Yb(2)–O(6,10,12) lying between 3.855 and 4.866 Å). As a consequence, the coordination number of the Yb(2) cations increases up to eight, and the coordination environment is a distorted square antiprism, as with the Yb(1) atom. It should be noted that the Topos program[45] confirms the Yb(2)···O(8) interaction. Moreover, two terminal ligands are twisted in a butterfly style. The dihedral angles between benzene rings connected with oxygen atoms are equal to 55.17 and 47.21°.

The bridging ligand is not planar as well. The Yb–O and Yb–N distances vary in the ranges of 2.1724(18)–2.3466(17) and 2.455(2)–2.515(2) Å, respectively. The Yb···Yb distance is 3.78559(18) Å. These geometrical parameters are in accordance with those reported for the related $[(CH_3OH)Yb_2L_3]$ compound.[44] Selected bond lengths and angles are summarized in Table 1.

Photophysical properties

UV-vis absorption spectra of H_2L and **1–5** were obtained in a MeCN solution at 2×10^{-5} M. The Schiff-base showed a π–π* band peaked at 280 nm, whereas the zinc dimer **1** revealed an additional strong broad band assigned to the LMCT in the 370–500 nm region. Binding of the ZnL chromophore to Yb $[OCH(CF_3)_2]_3$ caused a hypsochromic shift of the LMCT band

Table 1 Selected interatomic distances [Å] and bond angles [°] for complexes **1–4**

1			
Zn(2)–O(10)	1.958(2)	O(10)–Zn(2)–O(12)	95.07(8)
Zn(2)–O(12)	2.030(2)	O(10)–Zn(2)–N(3)	91.88(9)
Zn(2)–N(3)	2.046(3)	O(12)–Zn(2)–N(3)	167.18(9)
Zn(2)–N(4)	2.073(2)	O(10)–Zn(2)–N(4)	157.39(9)
Zn(2)–O(12A)	2.1180(19)	O(12)–Zn(2)–N(4)	88.97(9)
Zn(2)–Zn(2A)	2.9913(7)	N(3)–Zn(2)–N(4)	80.57(10)
2			
Zn(1)–O(8)	2.002(2)	O(2)–Zn(1)–O(3)	77.73(8)
Zn(1)–O(2)	2.028(2)	O(2)–Zn(1)–N(2)	142.27(9)
Zn(1)–O(3)	2.036(2)	O(3)–Zn(1)–N(2)	88.10(9)
Zn(1)–N(2)	2.065(2)	O(2)–Zn(1)–N(1)	88.07(9)
Zn(1)–N(1)	2.065(2)	O(3)–Zn(1)–N(1)	138.45(9)
Yb(1)–O(7)	2.131(2)	N(2)–Zn(1)–N(1)	79.68(10)
Yb(1)–O(5)	2.132(2)	O(3)–Yb(1)–O(2)	67.29(7)
Yb(1)–O(6)	2.135(2)	O(3)–Yb(1)–O(4)	63.23(7)
Yb(1)–O(3)	2.293(2)	O(2)–Yb(1)–O(4)	130.41(7)
Yb(1)–O(2)	2.310(2)	O(3)–Yb(1)–O(1)	129.87(7)
Yb(1)–O(4)	2.547(2)	O(2)–Yb(1)–O(1)	62.59(7)
Yb(1)–O(1)	2.566(2)	O(4)–Yb(1)–O(1)	166.41(7)
Yb(1)–Zn(1)	3.4581(3)		
3			
Zn(1)–O(5)	1.9291(15)	O(1)–Zn(1)–O(3)	77.00(6)
Zn(1)–O(1)	2.0111(14)	O(1)–Zn(1)–N(1)	89.33(6)
Zn(1)–O(3)	2.0270(14)	O(3)–Zn(1)–N(1)	141.05(6)
Zn(1)–N(1)	2.0449(17)	O(1)–Zn(1)–N(2)	143.98(6)
Zn(1)–N(2)	2.0474(17)	O(3)–Zn(1)–N(2)	88.41(6)
Zn(2)–O(11)	1.9336(15)	N(1)–Zn(1)–N(2)	81.62(7)
Zn(2)–O(9)	2.0207(14)	O(9)–Zn(2)–O(7)	76.41(6)
Zn(2)–O(7)	2.0263(14)	O(9)–Zn(2)–N(4)	88.63(6)
Zn(2)–N(4)	2.0550(17)	O(7)–Zn(2)–N(4)	135.94(6)
Zn(2)–N(3)	2.0575(17)	O(9)–Zn(2)–N(3)	143.57(7)
Yb(1)–O(6)	2.1053(15)	O(7)–Zn(2)–N(3)	87.66(6)
Yb(1)–O(13)	2.1590(14)	N(4)–Zn(2)–N(3)	80.35(7)
Yb(1)–O(14)	2.2150(14)	O(1)–Yb(1)–O(3)	67.20(5)
Yb(1)–O(1)	2.2684(14)	O(1)–Yb(1)–O(4)	131.37(5)
Yb(1)–O(3)	2.2744(14)	O(3)–Yb(1)–O(4)	64.19(5)
Yb(1)–O(4)	2.4912(14)	O(1)–Yb(1)–O(2)	63.29(5)
Yb(1)–O(2)	2.5502(14)	O(3)–Yb(1)–O(2)	130.40(5)
Yb(2)–O(12)	2.0895(15)	O(4)–Yb(1)–O(2)	165.25(5)
Yb(2)–O(14)	2.1692(14)	O(9)–Yb(2)–O(7)	67.00(5)
Yb(2)–O(13)	2.2356(14)	O(9)–Yb(2)–O(8)	131.62(5)
Yb(2)–O(9)	2.2625(14)	O(7)–Yb(2)–O(8)	64.62(5)
Yb(2)–O(7)	2.2727(14)	O(9)–Yb(2)–O(10)	63.72(5)
Yb(2)–O(8)	2.4796(14)	O(7)–Yb(2)–O(10)	130.22(5)
Yb(2)–O(10)	2.5173(14)	O(8)–Yb(2)–O(10)	163.61(5)
Zn(1)–Yb(1)	3.3415(2)		
Zn(2)–Yb(2)	3.3977(2)		
Yb(1)–Yb(2)	3.53628(12)		
4			
Yb(1)–O(3)	2.1759(18)	O(3)–Yb(1)–O(1)	80.81(7)
Yb(1)–O(1)	2.1910(17)	O(3)–Yb(1)–O(5)	150.37(6)
Yb(1)–O(5)	2.2747(17)	O(1)–Yb(1)–O(5)	79.60(6)
Yb(1)–O(7)	2.3078(17)	O(3)–Yb(1)–O(7)	87.62(6)
Yb(1)–N(2)	2.464(2)	O(1)–Yb(1)–O(7)	87.99(6)
Yb(1)–N(4)	2.480(2)	O(5)–Yb(1)–O(7)	69.72(6)
Yb(1)–N(1)	2.500(2)	O(9)–Yb(2)–O(11)	86.89(6)
Yb(1)–N(3)	2.515(2)	O(9)–Yb(2)–O(7)	121.43(6)
Yb(1)–Yb(2)	3.78559(18)	O(11)–Yb(2)–O(7)	150.46(6)
Yb(2)–O(9)	2.1724(18)	O(9)–Yb(2)–O(5)	161.47(6)
Yb(2)–O(11)	2.1799(17)	O(11)–Yb(2)–O(5)	81.47(6)
Yb(2)–O(7)	2.2776(17)	O(7)–Yb(2)–O(5)	68.99(6)
Yb(2)–O(5)	2.3466(17)	O(9)–Yb(2)–O(1S)	81.92(8)
Yb(2)–O(1S)	2.408(2)	O(11)–Yb(2)–O(1S)	81.10(7)
Yb(2)–N(5)	2.455(2)	O(7)–Yb(2)–O(1S)	93.89(7)
Yb(2)–N(6)	2.467(2)	O(5)–Yb(2)–O(1S)	82.07(7)
Yb(2)–O(8)	3.056(2)		

and enhanced the optical density in the range of favourable two-photon absorption for **2**. Interestingly, although the anionic isopropoxide moiety, but not aqua, occupies the axial position in the coordination polyhedron of the Zn atom in the heterometallic product **3**, the spectrum of **3** was virtually identical to that of **2**. In contrast, the spectral line shape of the homometallic derivative **4** had no explicit absorption shoulder in the range of interest (Fig. 5a, Table 2). Spectrum of **5** was similar to that reported by H. Wang *et al.*[46]

Excitation of the Schiff-base approximately at 300 nm produced blue fluorescence. The complexes **1–4** exhibited visible emission exclusively from the LMCT state under 380 nm irradiation under ambient conditions (Fig. 5b, Table 2), whereas **5** showed an additional signal of room temperature phosphorescence at 630 nm (Fig. S1†). PL spectra of the solids **2–4** perfectly matched their emission spectra in MeCN. On the contrary, the LMCT emission band for dissolved **1** and **5** underwent a remarkable blue shift as compared to the luminescence of the solid samples (Fig. S1†); apparently, this could be explained based on the solvation of the metal centres by the MeCN molecules. Short-wavelength excited (λ_{ex} ~260–355 nm) luminescence of **1–5** contained a blue fluorescence signal of moderate intensity along with a strong LMCT band (Fig. S2†) that manifests the incomplete $^1S_1 \rightarrow$ LMCT energy transfer. In addition to visible light, **2–4** generated NIR emission corresponding to the $^2F_{5/2} \rightarrow {}^2F_{7/2}$ transition of Yb^{3+} (Fig. 5c, Table 2). For each ytterbium complex, the NIR PL spectra measured in the solid state and MeCN solution (Fig. S3†) demonstrated a very similar Stark splitting referring to the effect of the electrostatic ligand field on the energies of the f orbitals. This implies that no major structural changes occur in the coordination environment of Yb atoms during the dissolution of **2–4**. Metal-centred emission decay for **2–4** (Fig. 5d, Table 2) was measured *via* time-resolved spectroscopy and fitted using a multi-exponential expression:

$$I(t) = \sum_{i=1}^{n} \alpha_i \exp(-t/\tau_i) + \beta.$$

It has been found that PL of **2** decays mono-exponentially with τ = 2.7 μs, whereas radiative relaxation for compounds **3** and **4** has a bi-exponential character due to energy exchange between two closely located luminescent centres in one molecule. Therefore, their PL kinetics were described by average lifetime (2.0 μs for **3** and 3.3 μs for **4**), which is given as follows:

$$\langle\tau\rangle = \frac{\sum_{i=1}^{n} \alpha_i \tau_i^2}{\sum_{i=1}^{n} \alpha_i \tau_i}.$$

Since the lifetime of 4f excited states of lanthanide complexes depends on the geometry and chemical composition of the nearest environment around Ln^{3+}, non-radiative relaxation introduced by ligands or free solvent molecules containing C–H or O–H oscillators, and Ln–Ln energy exchange, it is interesting to assess the contribution of these factors towards the PL decay. Coordination polyhedra of **2** and **3** are close to the D_{5h} point group containing 20 elements of symmetry and consist of seven oxygen atoms. Thus, two hydroxyl groups and Yb–Yb energy transfer in molecule **3** reduce the NIR PL decay time by 26%. The complex **4** has coordination polyhedra close to the

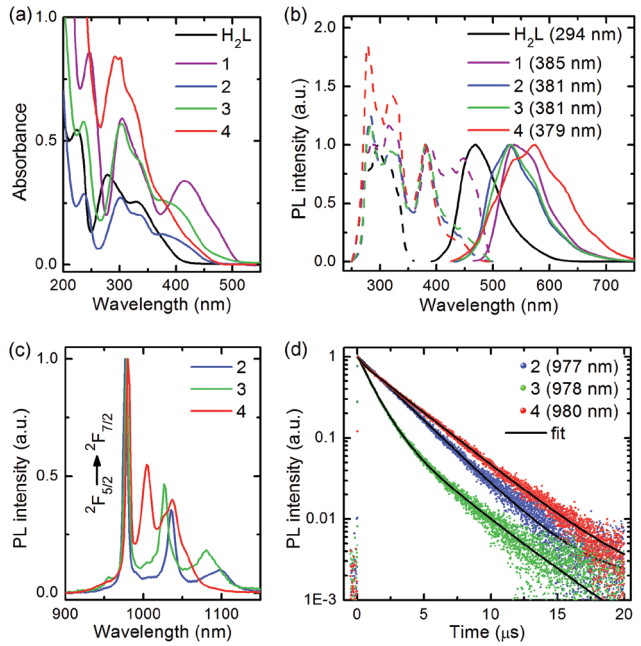

Fig. 5 UV-vis absorption (a) excitation and visible emission spectra (b) of free H_2L and complexes **1–4** in MeCN (concentration = 2 × 10^{-5} M) at room temperature. NIR PL of solids **2–4** (c) and their emission decay curves (d).

Table 2 Photophysical data of H_2L and complexes **1–4**

	λ_{abs} (nm)	λ_{ex} (nm)	λ_{em} [a] (nm)	τ_1, τ_2 [b] (μs)	$\langle\tau\rangle$ (μs)
H_2L	224, 280	295	470 (294)	—	—
1	245, 303, 415	284, 315, 385, 447	535 (385)	—	—
2	236, 301	283, 315, 381	529, 977, 1035, 1099 (381)	2.7 (1.0)	2.7
3	235, 302	283, 315, 381	531, 978, 1027, 1180 (381)	1.1 (0.83), 3.4 (0.17)	2.0
4	291	278, 322, 378	573, 980, 1004, 1037 (379)	3.3 (0.9), 3.7 (0.1)	3.3

[a] Excitation wavelength is given in parentheses. [b] Contribution of an exponential function with corresponding lifetime to overall PL decay is given in parentheses.

D_{2d} point group of order 16. On the one hand, the decrease in the number of symmetry elements shortens the lifetime of f–f emission since electrostatic field from lower symmetry coordination environment enforces the formation of mixed parity states of Ln^{3+}.[47] On the other hand, the presence of two and four N atoms in the polyhedra of **4**, contrary to the oxygen surroundings of Yb^{3+} in **2** and **3**, increases the decay time of metal-centred emission according to the data on the luminescence of Eu^{3+} benzimidazole-, benzoxazole-, and benzothiazole-substituted pyridine-2-carboxylates obtained by Bünzli and co-workers.[48–50] Considering that all the coordination polyhedra on the basis of their chemical inhomogeneity and/or distorted geometries could not be precisely described by the point groups, the impact of ligand-field symmetry on NIR PL decay of **2–4** is not pronounced. On the contrary, the chemical composition of the rare-earth centre surroundings, Yb–Yb energy exchange, and the presence of luminescence quenchers in the first coordination sphere of ytterbium atom have a significant influence on the observed radiative relaxation of the $^2F_{5/2}$ excited state.

To investigate the mechanism of sensitization of Yb^{3+} emission, energies of $^1S_1$ (≈28 570 cm^{-1}), LMCT (≈22 200 cm^{-1}), and $^3T_1$ (≈15 870 cm^{-1}) states of **2–4** were determined from the absorption spectra (Fig. 5a) and low-temperature phosphorescence of the Gd derivative (Fig. S4†). Efficient energy transfer process in lanthanide complexes occurs mostly *via* Förster or Dexter mechanisms, and there are two main conditions for its successful accomplishment: (i) spectral overlap (Ω_{DA}) between the ligand triplet state emission and rare-earth ion absorption and (ii) energy gap between $^3T_1$ and resonant level of Ln^{3+} exceeding 1500 cm^{-1}, which prevents backward lanthanide-to-ligand energy transfer.[51] Although the latter condition is fairly fulfilled for vast majority of Yb derivatives, there are numerous ytterbium complexes exhibiting NIR luminescence even in case of zero spectral overlap Ω_{DA}.[52–55] Taking into account that $\Delta E\{^3T_1 - {}^2F_{5/2}\} \approx 5400$ cm^{-1} for **2–4**, but the triplet state phosphorescence does not extend to wavelengths longer than 750 nm (Fig. S4†) in the region where Yb^{3+} absorbs light, it is surprising to find out the bright metal-centred PL of **2–4**. Therefore, a vanishing role of the triplet excited state in the ligand–ytterbium energy transfer was speculated and approved by measuring the luminescence intensity of the solid samples in the 77–373 K temperature range and in the experiments with aerated MeCN solutions. If the $^3T_1 \rightarrow Yb^{3+}*$ energy pathway is the most probable, the thermally activated non-radiative relaxation of the triplet state should weaken the f–f emission. Moreover, in the aerated solution, energy transfer from the $^3T_1$ state of the ytterbium complex towards the triplet oxygen molecule should give rise to noticeable oxygen-dependent behaviour of Yb^{3+} luminescence along with appearance of an additional peak at 1270 nm associated with emission of the produced singlet oxygen.[56] As expected, neither significant thermally/oxygen initiated changes in the PL spectra of the Yb complexes nor the signal of singlet oxygen were detected. These observations together with the fact that **2–4** generate f–f and LMCT emission attenuating and increasing synchronously under photoexcitation allow us to speculate that the $^2F_{5/2}$ state of Yb^{3+} ion is populated through reversible ligand-to-lanthanide electron transfer. In this process, an excited organic ligand (anionic or neutral) reduces Yb^{3+} to Yb^{2+} ion, and further, the radical ligand (neutral or cationic) oxidizes the divalent ytterbium, resulting in the formation of excited $Yb^{3+}*$ ion, which subsequently emits light.[55,57–60] An energy diagram describing the sensitization of luminescence of the complexes **2–5** is shown in the Fig. S5.†

To evaluate the influence of ZnL and $\{[(CF3)_2HCO]ZnL\}^-$ chromophore groups on the intensity of Yb^{3+} emission, luminescence spectra of **2–4** in MeCN (O.D. = 0.1 at 405 nm) were obtained under 405 nm laser diode excitation. Although the highest integral intensity was detected for $[(H_2O)Yb_2(L)_3]$ (**4**), the complex $\{(H_2O)Zn(\mu\text{-}L)Yb[OCH(CF_3)_2]_3\}$ (**2**) revealed an approximately three- and two-fold enhancement of the 980 nm band with respect to **3** and **4** (Fig. S3†). Therefore, taking into consideration that two-photon microscopes are usually equipped with silicon detectors having poor responsivity at wavelengths above 1000 nm, compound **2** is the best candidate for 2P microscopy among the ytterbium complexes studied herein.

Moreover, two-photon excitation (TPE) of NIR PL of the solids **2–4** was performed using a femtosecond Ti:Sa laser. An optimal excitation wavelength was chosen to be 750 nm because at longer wavelengths, the intrinsic one-photon absorption of Yb^{3+} began to obviously increase due to the strong Stark splitting of the $^2F_{5/2}$ and $^2F_{7/2}$ energy levels. The incident laser power varied from 1 to 100 mW. It was found that TPE at the LMCT absorption band produces desirable metal-centered emission of ytterbium ion at *ca.* 980 nm (Fig. 6a). The experimental data showing the dependence of the intensity of NIR PL on the incident laser power in the log–log scale nicely fit to the linear relationship with the slopes of 1.99 (**2**), 1.67 (**3**), and 1.63 (**4**) (Fig. 6b).

The complex **2** exhibited the most efficient two-photon excited luminescence; this is in line with the strong absorption of the 375 nm LMCT state of the ZnL chromophore, efficient ZnL → Yb^{3+} energy transfer, and absence of luminescence quenchers in the first coordination sphere of the Yb atom.

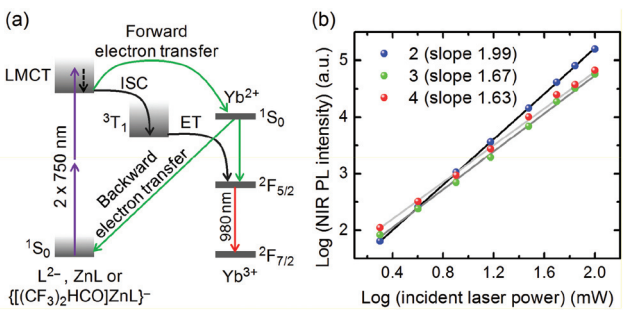

Fig. 6 Energy diagram describing the TPE metal-centred luminescence of the complexes **2–4** (a) and intensity of TPE NIR PL of **2–4** *versus* incident laser power relationship in the log–log scale (b).

Conclusions

In summary, five complexes: $[ZnL]_2$ (**1**), $\{(H_2O)Zn(\mu\text{-}L)Yb[OCH(CF_3)_2]_3\}$ (**2**), $\{[(CF_3)_2HCO]Zn(\mu\text{-}L)Yb[OCH(CF_3)_2](\mu\text{-}OH)\}_2$ (**3**), and $[(H_2O)Ln_2(L)_3]$ (Ln = Yb (**4**) and Gd (**5**)) were synthesized. The complexes **1–4** were structurally characterized. The ytterbium derivatives **2–4** showed bright NIR metal-centred luminescence under one- and two-photon excitation at the LMCT absorption band. The compound **2** exhibited the most efficient one- (λ_{ex} = 381 nm) and two-photon (λ_{ex} = 750 nm) excited f–f emission owing to substantial absorption of the LMCT state of the ZnL chromophore in the UV-to-vis spectral region, efficient ZnL → Yb^{3+} energy transfer, and absence of luminescence quenchers bound to the Yb atom. The moderate solubility of **2** in DMSO affords ground for its utilization in bioimaging.[11]

Acknowledgements

This work was supported by Russian Foundation for Basic Research (grant no. 16-33-00056). A.P.P. acknowledges financial support from Ministry of Education and Science of Russian Federation (Project 16.8939.2017/8.9) and Russian Foundation for Basic Research (grant no. 17-03-00621).

References

1 J. F. Herbst, *J. Magn. Magn. Mater.*, 1991, **100**, 57.
2 C. Kränkel, D.-T. Marzahl, F. Moglia, G. Huber and P. W. Metz, *Laser Photonics Rev.*, 2016, **10**, 548.
3 M. Nakazawa, *Opt. Rev.*, 2014, **21**, 862.
4 H. Xu, R. Chen, Q. Sun, W. Lai, Q. Su, W. Huang and X. Liu, *Chem. Soc. Rev.*, 2014, **43**, 3259.
5 S. V. Eliseeva and J.-C. G. Bunzli, *Chem. Soc. Rev.*, 2010, **39**, 189.
6 J.-C. G. Bunzli and S. V. Eliseeva, *New J. Chem.*, 2011, **35**, 1165.
7 M. Shang, C. Li and J. Lin, *Chem. Soc. Rev.*, 2014, **43**, 1372.
8 G. Piszczek, I. Gryczynski, B. P. Maliwal and J. R. Lakowicz, *J. Fluoresc.*, 2002, **12**, 15.
9 T. Zhang, X. Zhu, C. C. W. Cheng, W. M. Kwok, H. L. Tam, J. Hao, D. W. J. Kwong, W. K. Wong and K. L. Wong, *J. Am. Chem. Soc.*, 2011, **133**, 20120.
10 A. D'Aléo, A. Bourdolle, S. Brustlein, T. Fauquier, A. Grichine, A. Duperray, P. L. Baldeck, C. Andraud, S. Brasselet and O. Maury, *Angew. Chem., Int. Ed.*, 2012, **51**, 6622.
11 A. T. Bui, A. Grichine, S. Brasselet, A. Duperray, C. Andraud and O. Maury, *Chem. – Eur. J.*, 2015, **21**, 17757.
12 D. Zare, Y. Suffren, L. Guénée, S. V. Eliseeva, H. Nozary, L. Aboshyan-Sorgho, S. Petoud, A. Hauser and C. Piguet, *Dalton Trans.*, 2015, **44**, 2529.
13 R. Jia, H.-F. Li, P. Chen, T. Gao, W.-B. Sun, G.-M. Li and P.-F. Yan, *CrystEngComm*, 2016, **18**, 917.
14 L.-Y. Zhang, K. Li, M. Pan, Y.-N. Fan, H.-P. Wang and C.-Y. Su, *New J. Chem.*, 2016, **40**, 5379.
15 A. Chandra, K. Singh, S. Singh, S. Sivakumar and A. K. Patra, *Dalton Trans.*, 2016, **45**, 494.
16 F.-F. Chen, H.-B. Wei, Z.-Q. Bian, Z.-W. Liu, E. Ma, Z.-N. Chen and C.-H. Huang, *Organometallics*, 2014, **33**, 3275.
17 W.-K. Wong, X. Yang, R. A. Jones, J. H. Rivers, V. Lynch, W.-K. Lo, D. Xiao, M. M. Oye and A. L. Holmes, *Inorg. Chem.*, 2006, **45**, 4340.
18 W.-K. Lo, W.-K. Wong, W.-Y. Wong, J. Guo, K.-T. Yeung, Y.-K. Cheng, X. Yang and R. A. Jones, *Inorg. Chem.*, 2006, **45**, 9315.
19 W.-Y. Bi, X.-Q. Lü, W.-L. Chai, T. Wei, J.-R. Song, S.-S. Zhao and W.-K. Wong, *Inorg. Chem. Commun.*, 2009, **12**, 267.
20 W. Bi, T. Wei, X. Lü, Y. Hui, J. Song, S. Zhao, W.-K. Wong and R. A. Jones, *New J. Chem.*, 2009, **33**, 2326.
21 X. Yang, D. Schipper, A. Liao, J. M. Stanley, R. A. Jones and B. J. Holliday, *Polyhedron*, 2013, **52**, 165.
22 P. Chen, H. Chen, P. Yan, Y. Wang and G. Li, *CrystEngComm*, 2011, **13**, 6237.
23 W.-B. Sun, P.-F. Yan, S.-D. Jiang, B.-W. Wang, Y.-Q. Zhang, H.-F. Li, P. Chen, Z.-M. Wang and S. Gao, *Chem. Sci.*, 2016, **7**, 684.
24 T. D. Pasatoiu, A. M. Madalan, M. Zamfirescu, C. Tiseanu and M. Andruh, *Phys. Chem. Chem. Phys.*, 2012, **14**, 11448.
25 D. C. Bradley, J. S. Ghotra and F. A. Hart, *J. Chem. Soc., Dalton Trans.*, 1973, 1021.
26 D. M. Kuzyaev, T. V. Balashova, M. E. Burin, G. K. Fukin, R. V. Rumyantcev, A. P. Pushkarev, V. A. Ilichev, I. D. Grishin, D. L. Vorozhtsov and M. N. Bochkarev, *Dalton Trans.*, 2016, **45**, 3464.
27 *SAINT. Data Reduction and Correction Program. Version 8.37A*, Bruker AXS Inc., Madison, Wisconsin, USA, 2012.
28 *Data Collection. Reduction and Correction Program. Version 1.171.37.35*, CrysAlisPro – Software Package Agilent Technologies, 2012.
29 G. M. Sheldrick, *Acta Crystallogr., Sect. A*, 2015, **71**, 3.
30 G. M. Sheldrick, *SHELXTL, Version 2014/7, Structure Determination Software Suite*, Bruker AXS, Madison, WI, 2000.
31 G. M. Sheldrick, *SADABS-2014/5. Bruker/Siemens Area Detector Absorption Correction Program*, Bruker AXS Inc., Madison, Wisconsin, USA, 2001.
32 *SCALE3 ABSPACK: Empirical absorption correction*, CrysAlisPro – Software Package, Agilent Technologies, 2012.
33 D. M. Kuzyaev, R. V. Rumyantsev, G. K. Fukin and M. N. Bochkarev, *Russ. Chem. Bull.*, 2014, **63**, 848.
34 W.-Y. Bi, X.-Q. Lü, W.-L. Chai, J.-R. Song, W.-K. Wong, X.-P. Yang and R. A. Jones, *Z. Anorg. Allg. Chem.*, 2008, **634**, 1795.
35 D. Olea-Román, N. Bélanger-Desmarais, M. Flores-Álamo, C. Bazán, F. Thouin, C. Reber and S. E. Castillo-Blum, *Dalton Trans.*, 2015, **44**, 17175.
36 C. Yu, Z. Zhang, L. Liu, H. Li, Y. He, X. Lü, W.-K. Wong and R. A. Jones, *New J. Chem.*, 2015, **39**, 3698.
37 R. D. Shannon, *Acta Crystallogr., Sect. A: Cryst. Phys., Diffr., Theor. Gen. Cryst.*, 1976, **32**, 751.
38 S. S. Batsanov, *Russ. J. Inorg. Chem.*, 1991, **36**, 3015.

39 M. V. Escárcega-Bobadilla, G. A. Zelada-Guillén, S. V. Pyrlin, M. Wegrzyn, M. M. D. Ramos, E. Giménez, A. Stewart, G. Maier and A. W. Kleij, *Nat. Commun.*, 2013, **4**, 2648.
40 M. M. Belmonte, S. J. Wezenberg, R. M. Haak, D. Anselmo, E. C. Escudero-Adan, J. Benet-Buchholz and A. W. Kleij, *Dalton Trans.*, 2010, **39**, 4541.
41 C. Janiak, *J. Chem. Soc., Dalton Trans.*, 2000, 3885.
42 Yu. V. Zefirov and P. M. Zorky, *Russ. Chem. Rev.*, 1995, **64**, 415.
43 T. D. Pasatoiu, J.-P. Sutter, A. M. Madalan, F. Z. C. Fellah, C. Duhayon and M. Andruh, *Inorg. Chem.*, 2011, **50**, 5890.
44 T.-Q. Liu, P.-F. Yan, F. Luan, Y.-X. Li, J.-W. Sun, C. Chen, F. Yang, H. Chen, X.-Y. Zou and G.-M. Li, *Inorg. Chem.*, 2015, **54**, 221.
45 V. A. Blatov, A. P. Shevchenko and D. M. Proserpio, *Cryst. Growth Des.*, 2014, **14**, 3576.
46 H. Wang, C. Liu, T. Liu, S. Zeng, W. Cao, Q. Ma, C. Duan, J. Dou and J. Jiang, *Dalton Trans.*, 2013, **42**, 15355.
47 B. M. Walsh, Judd–Ofelt theory: principles and practices, in *Advances in Spectroscopy for Lasers and Sensing*, ed. B. Di Bartolo and O. Forte, Springer, Printed in the Netherlands, 2006, pp. 403–433.
48 N. M. Shavaleev, R. Scopelliti, F. Gumy and J.-C. G. Bünzli, *Inorg. Chem.*, 2009, **48**, 6178.
49 N. M. Shavaleev, R. Scopelliti, F. Gumy and J.-C. G. Bünzli, *Inorg. Chem.*, 2009, **48**, 5611.
50 N. M. Shavaleev, S. V. Eliseeva, R. Scopelliti and J.-C. G. Bünzli, *Chem. – Eur. J.*, 2009, **15**, 10790.
51 J.-C. G. Bünzli and S. V. Eliseeva, Photophysics of Lanthanoid Coordination Compounds, in *Comprehensive Inorganic Chemistry II*, ed. J. Reedijk and K. Poeppelmeier, vol. 8, Elsevier, Oxford, 2013, pp. 339–398.
52 S. Biju, Y. K. Eom, J.-C. G. Bunzli and H. K. Kim, *J. Mater. Chem. C*, 2013, **1**, 6935.
53 Z. Li, H. Zhang and J. Yu, *Thin Solid Films*, 2012, **520**, 3663.
54 C. Reinhard and H. U. Gudel, *Inorg. Chem.*, 2002, **41**, 1048.
55 V. A. Ilichev, A. P. Pushkarev, R. V. Rumyantcev, A. N. Yablonskiy, T. V. Balashova, G. K. Fukin, D. F. Grishin, B. A. Andreev and M. N. Bochkarev, *Phys. Chem. Chem. Phys.*, 2015, **17**, 11000.
56 A. Watkis, R. Hueting, T. J. Sørensen, M. Tropiano and S. Faulkner, *Chem. Commun.*, 2015, **51**, 15633.
57 W. D. Horrocks Jr., P. J. Bolender, W. D. Smith and R. M. Supkowski, *J. Am. Chem. Soc.*, 1997, **119**, 5972–5973.
58 T. Ala-Kleme, K. Haapakka and M. Latva, *Anal. Chim. Acta*, 1999, **395**, 205.
59 A. Y. Zhong, L. Si, H. He and A. G. Sykes, *Dalton Trans.*, 2011, **40**, 11389.
60 P. Pushkarev, V. A. Ilichev, T. V. Balashova, D. L. Vorozhtsov, M. E. Burin, D. M. Kuzyaev, G. K. Fukin, B. A. Andreev, D. I. Kryzhkov, A. N. Yablonskiy and M. N. Bochkarev, *Russ. Chem. Bull.*, 2013, **62**, 392.